Small Molecule Therapeutics

Molecular Cancer Therapeutics

PET Imaging of β-Glucuronidase Activity by an Activity-Based ^{124}I-Trapping Probe for the Personalized Glucuronide Prodrug Targeted Therapy

Yu-Cheng Su[1,2], Ta-Chun Cheng[3,4], Yu-Ling Leu[5], Steve R. Roffler[2], Jaw-Yuan Wang[6], Chih-Hung Chuang[7], Chien-Han Kao[3], Kai-Chuan Chen[2], Hsin-Ell Wang[8], and Tian-Lu Cheng[9,10,11]

Abstract

Beta-glucuronidase (βG) is a potential biomarker for cancer diagnosis and prodrug therapy. The ability to image βG activity in patients would assist in personalized glucuronide prodrug cancer therapy. However, whole-body imaging of βG activity for medical usage is not yet available. Here, we developed a radioactive βG activity–based trapping probe for positron emission tomography (PET). We generated a ^{124}I-tyramine–conjugated difluoromethylphenol beta-glucuronide probe (TrapG) to form ^{124}I-TrapG that could be selectively activated by βG for subsequent attachment of ^{124}I-tyramine to nucleophilic moieties near βG-expressing sites. We estimated the specificity of a fluorescent FITC-TrapG, the cytotoxicity of tyramine-TrapG, and the serum half-life of ^{124}I-TrapG. βG targeting of ^{124}I-TrapG *in vivo* was examined by micro-PET. The biodistribution of ^{131}I-TrapG was investigated in different organs. Finally, we imaged the endogenous βG activity and assessed its correlation with therapeutic efficacy of 9-aminocamptothecin glucuronide (9ACG) prodrug in native tumors. FITC-TrapG showed specific trapping at βG-expressing CT26 (CT26/mβG) cells but not in CT26 cells. The native TrapG probe possessed low cytotoxicity. ^{124}I-TrapG preferentially accumulated in CT26/mβG but not CT26 cells. Meanwhile, micro-PET and whole-body autoradiography results demonstrated that ^{124}I-TrapG signals in CT26/mβG tumors were 141.4-fold greater than in CT26 tumors. Importantly, Colo205 xenografts in nude mice that express elevated endogenous βG can be monitored by using infrared glucuronide trapping probes (NIR-TrapG) and suppressed by 9ACG prodrug treatment. ^{124}I-TrapG exhibited low cytotoxicity allowing long-term monitoring of βG activity *in vivo* to aid in the optimization of prodrug targeted therapy. *Mol Cancer Ther; 13(12); 2852–63. ©2014 AACR.*

[1]Institute of Microbiology and Immunology, National Yang-Ming University, Taipei, Taiwan. [2]Institute of Biomedical Sciences, Academia Sinica, Taipei, Taiwan. [3]Graduate Institute of Medicine, Kaohsiung Medical University, Kaohsiung, Taiwan. [4]Graduate Institute of Pharmacognosy, Taipei Medical University, Taipei, Taiwan. [5]Department of Pharmacy, Chia Nan University of Pharmacy and Science, Tainan, Taiwan. [6]Department of Surgery, Faculty of Medicine, College of Medicine, Kaohsiung Medical University, Kaohsiung, Taiwan. [7]Institute of Basic Medical Sciences, National Cheng Kung University, Tainan, Taiwan. [8]Department of Biomedical Imaging and Radiological Sciences, National Yang-Ming University, Taipei, Taiwan. [9]Institute of Biomedical Sciences, National Sun Yat-Sen University, Kaohsiung, Taiwan. [10]Department of Biomedical Science and Environmental Biology, Kaohsiung Medical University, Kaohsiung, Taiwan. [11]Center for Biomarkers and Biotech Drugs, Kaohsiung Medical University, Kaohsiung, Taiwan.

Note: Supplementary data for this article are available at Molecular Cancer Therapeutics Online (http://mct.aacrjournals.org/).

Y.-C. Su and T.-C. Cheng contributed equally to this article.

Corresponding Authors: Tian-Lu Cheng, Department of Biomedical and Environmental Biology, Kaohsiung Medical University, 100 Shih-Chuan 1st Road, Kaohsiung, Taiwan. Phone: 886-7-3121101, ext. 2360; Fax: 886-7-3227508; E-mail: tlcheng@kmu.edu.tw; and Hsin-Ell Wang, Department of Biomedical Imaging and Radiological Sciences, National Yang-Ming University, No. 155, Sec. 2, Li-Nong Street, Taipei, Taiwan. Phone: 886-2-28267215; Fax: 886-2-28201095; E-mail: hewang@ym.edu.tw

doi: 10.1158/1535-7163.MCT-14-0212

Introduction

β-Glucuronidase (βG) can catalyze the hydrolysis of β-D-glucuronic acid residues for the breakdown of mucopolysaccharides (e.g., heparan sulfate) in lysosomes (1). It has been widely used as an attractive enzyme for reporter imaging (2–4) and cancer prodrug therapies (5–8). Several glucuronide prodrugs have been used in antibody-directed enzyme prodrug therapy (ADEPT; refs. 9–11) and gene-directed enzyme prodrug therapy (GDEPT; refs. 6, 12, 13) as well as directly in prodrug monotherapy, which relies on the elevated levels of βG found in the tumor microenvironment (14–16) to selectively convert prodrug into active drug. For instance, Albin and colleagues reported that the level of βG human breast tumors was up to 6-times greater than that in normal tissues (17). Sperker and colleagues also reported that pancreatic adenocarcinoma exhibited higher βG levels than did normal pancreatic tissue (14). Furthermore, human tumor xenografts also showed elevated levels of βG, including human breast (MCF-7, BT20, and HS578T), colon (HT29 and SW480), and small-cell lung cancer (OH3 and SW2) cell

Published OnlineFirst October 2, 2014; DOI: 10.1158/1535-7163.MCT-14-0212

lines (18). Elevated levels of βG present in the tumor environment are believed to be due to tumor overexpression (14) and release from necrotic tumor tissues (19) or tumor-infiltrating immune cells (15). Because βG has been considered as a tumor marker (14, 15, 20), it would be very useful to image βG activity *in vivo* to personalize glucuronide prodrug treatment and greatly improve exogenous or endogenous βG-based targeted therapy.

We have previously demonstrated that a fluorescein di-β-D-glucuronide probe (FDGlcU) can be applied for the assessment of βG activity *in vivo*. However, the fluorescent product FDGlcU rapidly leaked from βG-expressing sites and exhibited poor penetrative properties, limiting imaging to subcutaneous tumors but not deeper tumors (2). To overcome these problems, we also developed fluorescent glucuronide trapping probes by conjugating a fluorescein isothiocyanate (FITC; λex = 495 nm, λem = 519 nm) and the near infrared dye IR-820 isothiocyanate (NIR; λex = 710 nm, λem = 820 nm) with the difluoromethylphenol beta-glucuronide trapping moiety to form FITC-TrapG and NIR-TrapG probes, respectively. Only the highly signal penetrating NIR-TrapG with near infrared spectrum properties can be used in long-term tracking (for about 72 hours) of βG activity in deep liver tissues; the FITC-TrapG cannot be. NIR-TrapG is a good probe to monitor the βG activity in small animals (21) but the near infrared fluorescent probes are still not feasible for human use as the large thickness of the human body causes a decrease in fluorescence emission and optical imaging systems for medical usage are not available. Development of a positron emission tomography (PET) glucuronide probe to image βG activity will provide a novel method to allow optimization of the protocols for βG-based personalized cancer therapy. Indeed, we previously described a ^{124}I-phenolphthalein-glucuronide probe (^{124}I-PTH-G) to image βG activity *in vivo* by micro-PET (3). The conversion of ^{124}I-PTH-G by βG caused the *in situ* precipitation of ^{124}I-PTH due to its hydrophobic property. However, this probe only allows short-term *in vivo* imaging (about 3 hours) and may induce carcinogenesis based on a feed study of phenolphthalein in B6C3F$_1$ mice and F344/N rats (22).

In the present study, we developed a ^{124}I-tyramine-difluoromethylphenol-glucuronide probe (^{124}I-TrapG) for imaging βG activity by micro-PET. ^{124}I-TrapG can be converted by βG to form the quinine methide derivative of ^{124}I-Trap to quickly react with any nearby nucleophile moiety such as membrane proteins (23) (Fig. 1B). The specificity of the probe was tested *in vitro* by incubating a FITC-TrapG probe with either CT26/mβG (CT26 cancer cells engineered to express membrane-anchored βG) or parental CT26 cells. The specificity and cytotoxicity of TrapG were also examined by incubating the probe with CT26/mβG or CT26 cells. For *in vivo* imaging studies, the ^{124}I-TrapG was injected into mice bearing both CT26/mβG and parental CT26 tumors to assess intratumoral βG activity by micro-PET. We also examined the biodistribution of ^{124}I-TrapG in various tissues. To estimate whether TrapG probes can be used to detect endogenous βG activity *in vivo*, immunodeficient mice bearing Colo205 (human βG^{high}) and SW620 (human βG^{low}) tumors were injected with NIR-TrapG for optical imaging. Finally, to evaluate whether the endogenous βG can specifically activate glucuronide prodrugs, mice bearing Colo205 or SW620 tumors were injected with 9-aminocamptothecin glucuronide (9ACG) for βG-mediated prodrug therapy. 9ACG is a water-soluble substrate of βG that displays antineoplastic activity after being hydrolyzed by βG to release a topoisomerase I inhibitor, 9AC. Our results indicate that ^{124}I-TrapG can systemically image the location and the expression of βG *in vitro* and *in vivo*, promoting βG usage as a reporter gene for future clinical therapy protocols.

Materials and Methods

Reagents, cells, and mice

The 9ACG was synthesized as described (24). D-saccharic acid 1,4-lactone monohydrate (SAL) was purchased from Sigma-Aldrich. We previously generated CT26/mβG cells (2) in 2007. CL1-5 cells (25) were obtained from Dr. Cheng-Wen Wu's laboratory (Institute of Biomedical Sciences, Academia Sinica, Taipei, Taiwan) in 2003. CT26, SW480, Hela, HCC36, SW620, and Colo205 cells were obtained from ATCC (American Type Culture Collection) in 2002. All these cell lines were maintained in Dulbecco's minimal essential medium (DMEM; Sigma-Aldrich) supplemented with 10% heat-inactivated bovine calf serum, 100 U/mL penicillin and 100 μg/mL streptomycin at 37°C in an atmosphere of 5% CO_2. The cell lines were not authenticated by our laboratory. All cell lines were propagated for less than 6 months after resuscitation. Six- to 8-week-old female BALB/cByJNarl and BALB/cAnN.Cg-Foxn1^{nu}/CrlNarl (BALB/c nude) mice were purchased from the National Laboratory Animal Center, Taipei, Taiwan. Mice were pretreated with 0.2% Lugol solution (Sigma-Aldrich) in their drinking water for 2 days before injection of radioiodinated probes, as previously described (3) to reduce thyroid uptake. All animal experiments were conducted in specific pathogen-free conditions and in accordance with guidelines approved by the Animal Care and Use Committee of the National Yang-Ming University.

Radioiodination of ^{131}I or ^{124}I-TrapG

Compound 5 shown in Supplementary Methods (Tyramine-TrapG) was labeled with iodine 124 (^{124}I) NaI (3.7–37 MBq; IBA Molecular) or ^{131}I NaI solution (Nuclear Science and Technology Development Center, National Tsing Hua University, Taiwan) using chloramine-T methods as previously described (3). The specific activity of ^{131}I-TrapG and ^{124}I-TrapG were about 500 MBq/mol with > 95% purity as determined by radio-thin-layer chromatography. The radiochemical yields of ^{131}I-TrapG and ^{124}I-TrapG were 65% and 70%, respectively.

Published OnlineFirst October 2, 2014; DOI: 10.1158/1535-7163.MCT-14-0212

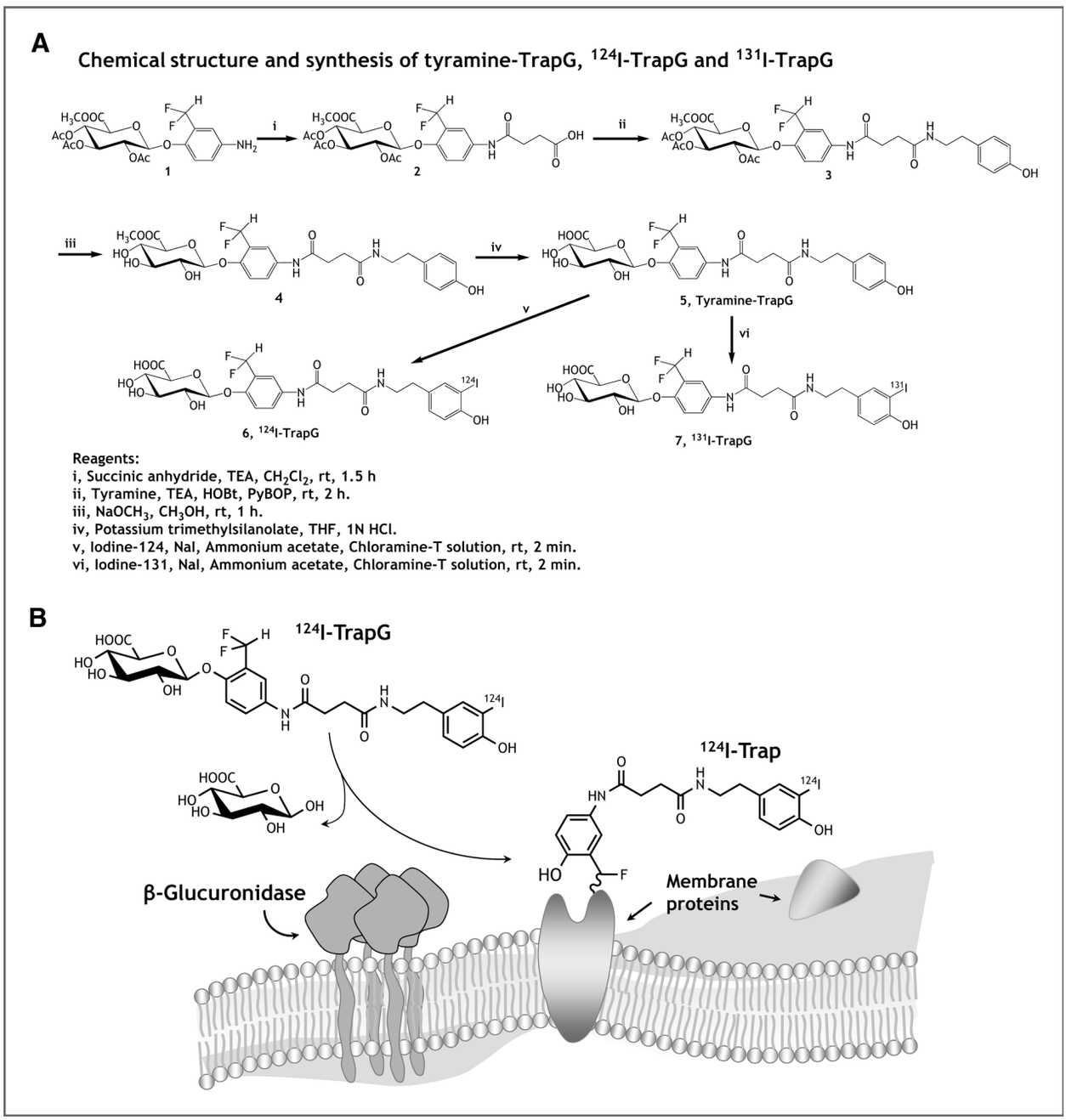

Figure 1. Chemical synthesis and βG-mediated activation of tyramine-TrapG probes. A, chemical structure and synthesis of ^{131}I-TrapG and ^{124}I-TrapG probes. B, βG-mediated activation of the ^{124}I-TrapG probe releases the ^{124}I-difluoromethylphenol moiety that may cross-link nucleophiles near the site of βG expression *in vitro* and *in vivo*.

Analysis of cell surface trapping of FITC-TrapG probe

CT26 and CT26/mβG cells were stained with 0.5 μmol/L FITC-TrapG probes in serum-free PBS (pH = 6.5) in the presence or absence of SAL (0.5 mg/mL) for 30 minutes at 37°C. Unreactive probes were removed by washing with cold PBS twice. The surface fluorescence of 10^4 viable cells was measured on a BD LSR II Flow Cytometer (Becton Dickinson) and analyzed with FlowJo (TreeStar). Similarly, cells (3×10^5 cells) were incubated with 0.69 μmol/L FITC-TrapG in pH 6.5 PBS for 45 minutes at room temperature. The cells were boiled in reducing SDS buffer, electrophoresed on a SDS-PAGE, and transferred to PVDF membranes. Membranes were sequentially stained with mouse anti-FITC antibody followed by HRP-conjugated goat anti-mouse antibody (Jackson ImmunoResearch

Published OnlineFirst October 2, 2014; DOI: 10.1158/1535-7163.MCT-14-0212

Laboratories). Bands were visualized by ECL detection (Thermo Scientific).

Cytotoxicity of the TrapG probe

Graded concentrations of Tyramine-TrapG or the glucuronide prodrug (p-hydroxyaniline mustard glucuronide, BHAMG; ref. 7) were added to the CT26 cells (1×10^4 cells per well) with or without recombinant *E. coli* β-glucuronidase (eβG; 2 μg/well) at 37°C for 24 hours. 37 kBq ^{3}H-thymidine was added to the cells during the last 12-hour period of culture. Results are expressed as percentage of ^{3}H-thymidine incorporation as compared with untreated cells by the following formula:

$$\%\ \text{of Control} = 100 \times (\text{cpm sample} - \text{cpm background}) / (\text{cpmcontrol} - \text{cpmbackground})$$

The specificity of ^{124}I-TrapG

Graded concentrations of ^{124}I-TrapG in PBS were added to the CT26 and CT26/mβG cells (8×10^4 cells per well) at room temperature for 1 hour. Likewise, the cells were incubated with 0.74 MBq of ^{124}I-TrapG for various times, following washing with PBS (supplemented with 0.495 mmol/L $MgCl_2$ and 0.9 mmol/L $CaCl_2$, pH = 3.0) to remove nonbound probe. The radioactivity of the cells was measured in a 1470 Wizard gamma counter (Wallac).

Liver function evaluation

Groups of BALB/c mice ($n = 6$) were i.v. injected with PBS or 40 mg/kg TrapG probes. Blood was collected in serum separation 7 days postinjection. Liver injury was assessed by measuring serum aspartate aminotransferase (AST), alanine aminotransferase (ALT), and total bilirubin (TBIL) levels using a Fuji Dri-Chem 3500 biochemistry analyzer (Fujifilm).

Serum half-life of ^{124}I-TrapG probe

BALB/c mice ($n = 3$) were i.v. injected with 1.85-MBq ^{124}I-TrapG, and blood samples were collected at different time points. The blood samples were weighed and assayed for radioactivity in a gamma counter. The radioactivity in the samples is expressed as the percentage of injected dose per gram of tissue. The elimination half-life ($t_{1/2}$) of ^{124}I-TrapG was calculated by a two-phase exponential decay equation with use of software (Prism 4; Graphpad Software).

Imaging of βG activity *in vivo*

BALB/c mice ($n = 3$) bearing 200 mm^3 CT26/mβG (right hind leg) and control CT26 (left hind leg) tumors were i.v. injected with 3.7 MBq of ^{124}I-TrapG. The whole-body micro-PET imaging of pentobarbital-anesthetized mice was performed at 1, 8, and 20 hours postinjection using a micro-PET R4 scanner (Concorde Microsystems). To test the specificity of ^{124}I-TrapG *in vivo*, the mice were i.p. injected with SAL inhibitors (1 g per kilogram of body weight) 1 hour before ^{124}I-TrapG injection. Fully 3-dimensional list-mode data were collected using an energy window of 350 to 750 keV and a time window of 6 nanoseconds. Image pixel size was 0.85 mm transaxially with a 1.21 mm slice thickness. BALB/c nude mice ($n = 3$) bearing 100 mm^3 SW480, SW620, and Colo205 tumors or CL1-5, Hela, and HCC36 tumors were also i.v. injected with 100 μg of NIR-TrapG (21). Whole-body optical images were acquired on an IVIS Spectrum imaging system (Caliper Life Sciences) at 24 hours after probe injection at an acquisition time of 10 seconds.

In vivo antitumor activity

Groups of 5 BALB/c nude mice bearing 100 mm^3 subcutaneous SW620 and Colo205 tumors in their right flank were i.p. injected with doses of 50 mg/kg 9ACG or PBS on days 1, 3, and 6. Tumor volumes were measured every 2 to 3 days. Tumor sizes were calculated according to the formula: length × width × height × 0.5. The relative tumor volume was determined as: % = 100% Í (tumor size/initial tumor size).

Whole-body autoradiography in mice

Mice ($n = 3$) were i.v. injected with 1.85 MBq of ^{131}I-TrapG 3 hours before the mice were sacrificed by means of chloroform inhalation. Animals were dipped into isopentane at liquid nitrogen temperatures and embedded on a cryostat holder (7 × 5 cm) in 4% carboxylmethylcellulose. The frozen carcass was sliced into 30-μm whole-body sections then attached on microscopic slides. The whole-body sections were applied to an imaging plate (BAS cassette 2040; Fujifilm). After 36 hours of exposure, the phosphor images were acquired with a FLA5000 reader (Fujifilm).

Biodistribution of the radioiodinated TrapG probe

BALB/c mice ($n = 4$) bearing established CT26 and CT26/mβG tumors (200 mm^3) on the right and left shoulders, respectively, were i.v. injected with 1.85 MBq of ^{131}I-TrapG. The mice were sacrificed at 1, 8, 20, and 40 hours postinjection, and the radioactivity in selected tissues was measured in a multichannel gamma counter. The biodistribution of the probe was expressed as percentage of injected dose per gram tissue. The tumors were harvest at 20 hours after ^{124}I-TrapG injection then embedded in tissue embedding medium (Tissue-Tek O.C.T.) at −80°C, and sectioned into 5-μm slices. Consecutive sections were either directly placed onto a phosphor imaging plate for autoradiography and detected by Typhoon 9410 phosphorimager (GE Healthcare Life Sciences) or stained with the β-glucuronidase Reporter Gene Staining Kit (Sigma-Aldrich) as previously described (21).

Reverse transcription polymerase chain reaction

SW620 and Colo205 tumor tissue samples from tumor-bearing nude mice were snap frozen in liquid nitrogen before grinding the samples into fine powder. Total RNA

Published OnlineFirst October 2, 2014; DOI: 10.1158/1535-7163.MCT-14-0212

was extracted by using the NucleoSpin RNA Isolation Kit (MACHEREY-NAGEL) according to the manufacturer's protocol. Five micrograms of total RNA was reverse transcribed by using the SuperScript III RT-PCR system with oligo(dT) primers (Invitrogen). Two microliters of cDNA sample was amplified by PCR and visualized on an agarose gel. The primers 5′-TCACCCAAGAAGCAGCCCTTC-3′ and 5′-CTAGCTGGAAATGTTCGCTGC-3′ for mouse βG; 5′-CTGGCGCTGCCGCAGTTCTTCAA-3′ and 5′-GGTGAAACCCTGCAATCGTT-3′ for human βG; 5′-GACCACAGTCCATGCCATCACT-3′ and 5′-TCCACCACCCTGTTGCTGTAG-3′ for human GAPDH genes were used in PCR.

Results

Synthesis of ^{131}I-TrapG and ^{124}I-TrapG

The synthesis of ^{131}I-TrapG and ^{124}I-TrapG are shown in Fig. 1A. Methyl 1-O-(2-diflоromethyl-4-amino)-2,3,4-tri-O-acetyl-β-D-glucopyranuronate (**1**) was prepared as described previously (21). To prepare of Tyramine-TrapG, tyramine was coupled with compound **1** via an amide linkage to obtain compound **3**. The acetyl groups in **3** were removed by treatment with sodium methoxide and the methyl ester was changed to carboxylic acid via methyl trimethylsilanoate in 1 N hydrochloric acid to give compound **5**, Tyramine-TrapG. To prepare ^{131}I-TrapG and ^{124}I-TrapG, Tyramine-TrapG was labeled with iodine 124 (^{124}I) NaI or ^{131}I NaI solution and purified on a Sep-Pak PLus C18 cartridge. Details of synthesis are described in Supplementary Methods.

The specificity of the TrapG probe in βG-expressing cells

To examine whether the activated TrapG probes could be specifically trapped on βG-expressing cells, parental CT26 and CT26/mβG cells (CT26 cells engineered to express membrane-tethered βG on their surface, 93 kDa) were stained with 0.5 μmol/L FITC-TrapG probes in the presence or absence of SAL inhibitors. After washing with PBS, FITC that remained attached to cells was detected on a flow cytometer. As shown in Fig. 2A, CT26/mβG cells were specifically bound to FITC-TrapG probes in the absence of SAL inhibitors as compared with the CT26 cells. Meanwhile, the addition of SAL inhibitors completely suppressed the fluorescence retained by CT26/mβG, indicating that the activation of FITC-TrapG depended on βG activity (Fig. 2A). To verify that TrapG could be covalently cross-linked to the cell surface after reaction with βG, FITC-TrapG was added to CT26 or CT26/βG cells and analyzed by anti-FITC Western blot. Compared with the control cells, only CT26/mβG samples showed bands that were detected by anti-FITC antibodies, consistent with covalently cross-linking of FITC to the cell surface proteins as noncovalently bound FITC would dissociate from proteins boiled in reducing SDS-PAGE electrophoresis buffer (Fig. 2B). We conclude that activated FITC-Trap can covalently label bystander nucleophiles on βG-expressing cells.

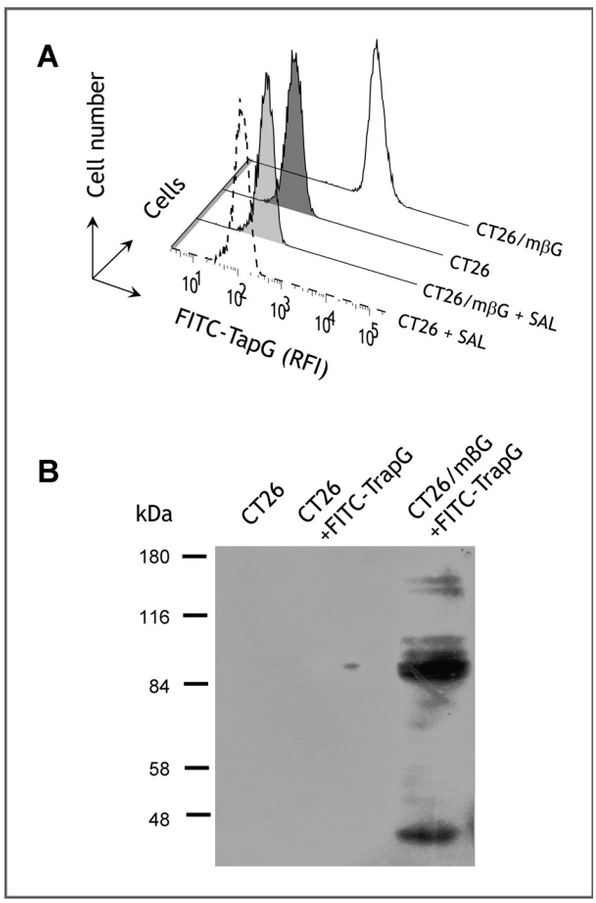

Figure 2. Specificity of the FITC-TrapG probe. A, functional binding of FITC-TrapG probes on CT26 and CT26/mβG cells was detected by flow cytometry after staining the cells with FITC-TrapG probes with or without SAL inhibitors. B, cell lysates prepared from CT26 or CT26/mβG cells that were treated with FITC-TrapG were electrophoresed on a SDS-PAGE and immunoblotted with the anti-FITC antibody.

Toxicity, specificity, and half-life of the TrapG probe

To estimate the cytotoxicity of TrapG to cells, graded concentrations of tyramine-TrapG and BHAMG (an anticancer glucuronide prodrug as positive control) were added to CT26 cells with or without the addition of 2 μg eβG. The incorporation of ^{3}H-thymidine into cellular DNA was measured as an index of cell viability. Figure 3A shows that 200 μmol/L tyramine-TrapG and BHAMG were not cytotoxic to CT26 cells in absence of βG. In the presence of βG, tyramine-TrapG displayed some toxicity at concentrations greater than about 100 μmol/L, whereas BHAMG was much more cytotoxic with an IC_{50} value of about 5 μmol/L. These results indicate that native tyramine-TrapG exhibited low cytotoxicity to cells with or without βG activation.

To examine the specificity of ^{124}I-TrapG, CT26/mβG or CT26 cells were incubated with graded concentrations

Published OnlineFirst October 2, 2014; DOI: 10.1158/1535-7163.MCT-14-0212

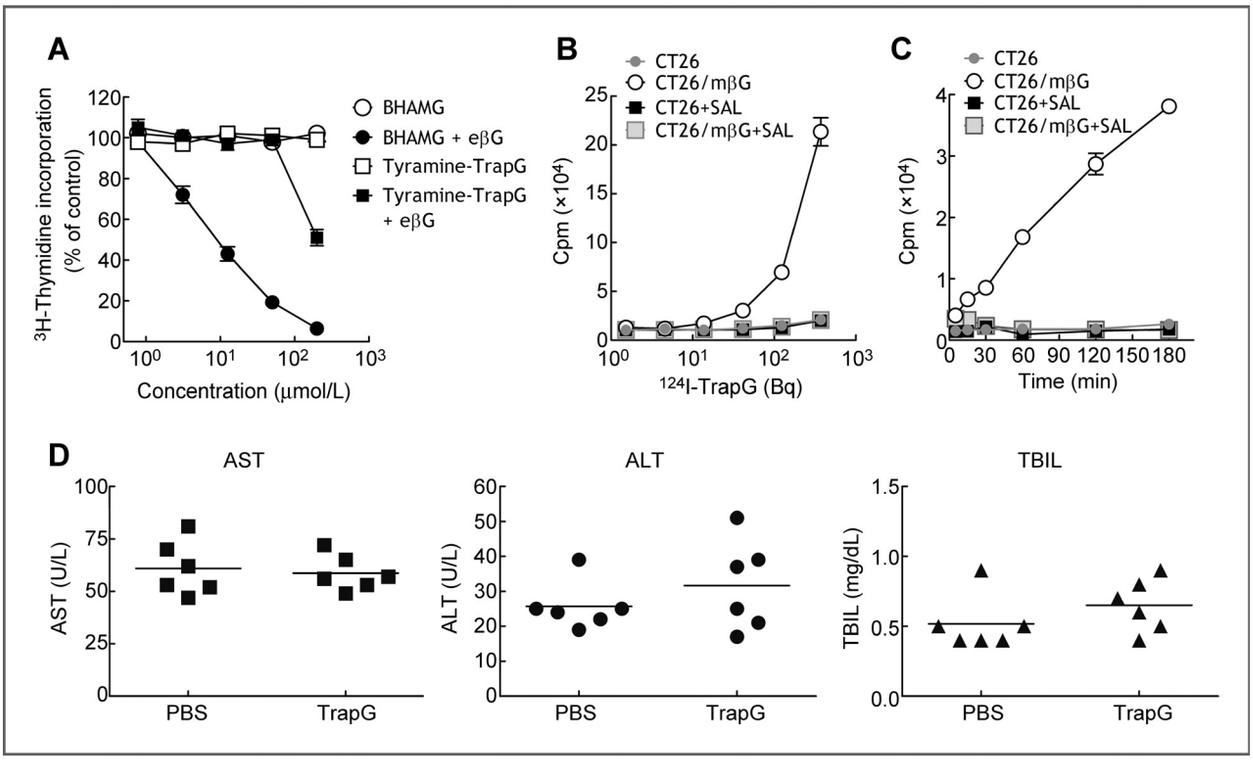

Figure 3. Cytotoxicity and specificity of TrapG. A, CT26 cells were incubated with graded concentrations of BHAMG (○), BHAMG with eβG (●), tyramine-TrapG (□), or tyramine-TrapG with eβG (■) for 72 hours. Cell viability was measured by determining incorporation of ^{3}H-thymidine into cellular DNA. B, graded concentrations of ^{124}I-TrapG were incubated with CT26 cells (●), CT26/mβG cells (○), CT26 cells with SAL (■), or CT26/mβG cells with SAL (■) for 60 minutes before the cells were washed and bound radioactivity was measured. C, 0.74 MBq/mL of ^{124}I-TrapG (50 μL/well) was incubated with CT26 cells (●), CT26/mβG cells (○), CT26 cells with SAL (■), or CT26/mβG cells with SAL (■) for the indicated times (5, 15, 30, 60, 120, and 180 minutes). The radioactivity of ^{124}I-TrapG treated cells was measured on a gamma counter. Results represent the mean of results from three separate wells. Mean ± SD. D, Balb/c mice were i.v. injected with 40 mg/kg PBS or TrapG. The serum concentrations of AST (■), ALT (●), and TBIL (▲) were measured 7 days after TrapG administration. Bars, SD ($n = 6$).

of ^{124}I-TrapG in the presence or absence of the βG inhibitor SAL. In addition, the cells were also incubated with ^{124}I-TrapG for different time periods. After washing cells with acidic PBS buffer, the radioactivity retained on the cells was measured on a gamma counter. Figures 3A and B show that addition of SAL completely blocked the radioactivity retained by cells expressing membrane-tethered βG, showing that the activation of ^{124}I-TrapG depended on βG activity. In addition, the radioactivity (cpm) retained by CT26/mβG cells after washing with acid PBS was 1.6 to 10.3-fold higher than CT26 cells and was both dose and time dependent (Fig. 3B and 3C). These results indicate that ^{124}I-TrapG could be selectively activated by βG, resulting in covalent retention of ^{124}I-TrapG at βG-expressing cells.

To investigate the toxicity of TrapG probes *in vivo*, mice were i.v. injected with tyramine-TrapG (40 mg/kg) or PBS. The blood samples were collected and analyzed to evaluate the hematologic parameters 7 days after tyramine-TrapG injection. The liver injury was determined by measuring the serum concentrations of AST, ALT, and TBIL. As shown in Fig. 3D, when compared with the PBS-treated mice, the serum levels of AST ($P = 0.37$), ALT ($P = 0.19$), and TBIL ($P = 0.93$) in tyramine-TrapG–treated mice were not significantly increased. These results suggest that tyramine-TrapG did not provoke hepatic toxicity *in vivo*.

To evaluate the pharmacokinetics of ^{124}I-TrapG, BALB/c mice were i.v. injected with ^{124}I-TrapG and the radioactivity in serum samples collected at defined times was measured on a gamma counter. Figure 4A shows that ^{124}I-TrapG elimination from the blood followed two-phase exponential decay kinetics, with an initial half-life of 7.3 minutes and a terminal half-life of 57.3 minutes.

Micro-PET imaging of βG activity in forced βG-overexpressing tumors with ^{124}I-TrapG

To evaluate whether ^{124}I-TrapG could serve as a micro-PET probe for imaging βG-expressing tumors *in vivo*, BALB/c mice ($n = 3$) bearing established subcutaneous CT26/mβG and control CT26 tumors were i.v. injected with ^{124}I-TrapG for micro-PET imaging at 1, 8, and 20 hours after probe injection. Enhanced signals of ^{124}I-TrapG were observed in CT26/mβG

Published OnlineFirst October 2, 2014; DOI: 10.1158/1535-7163.MCT-14-0212

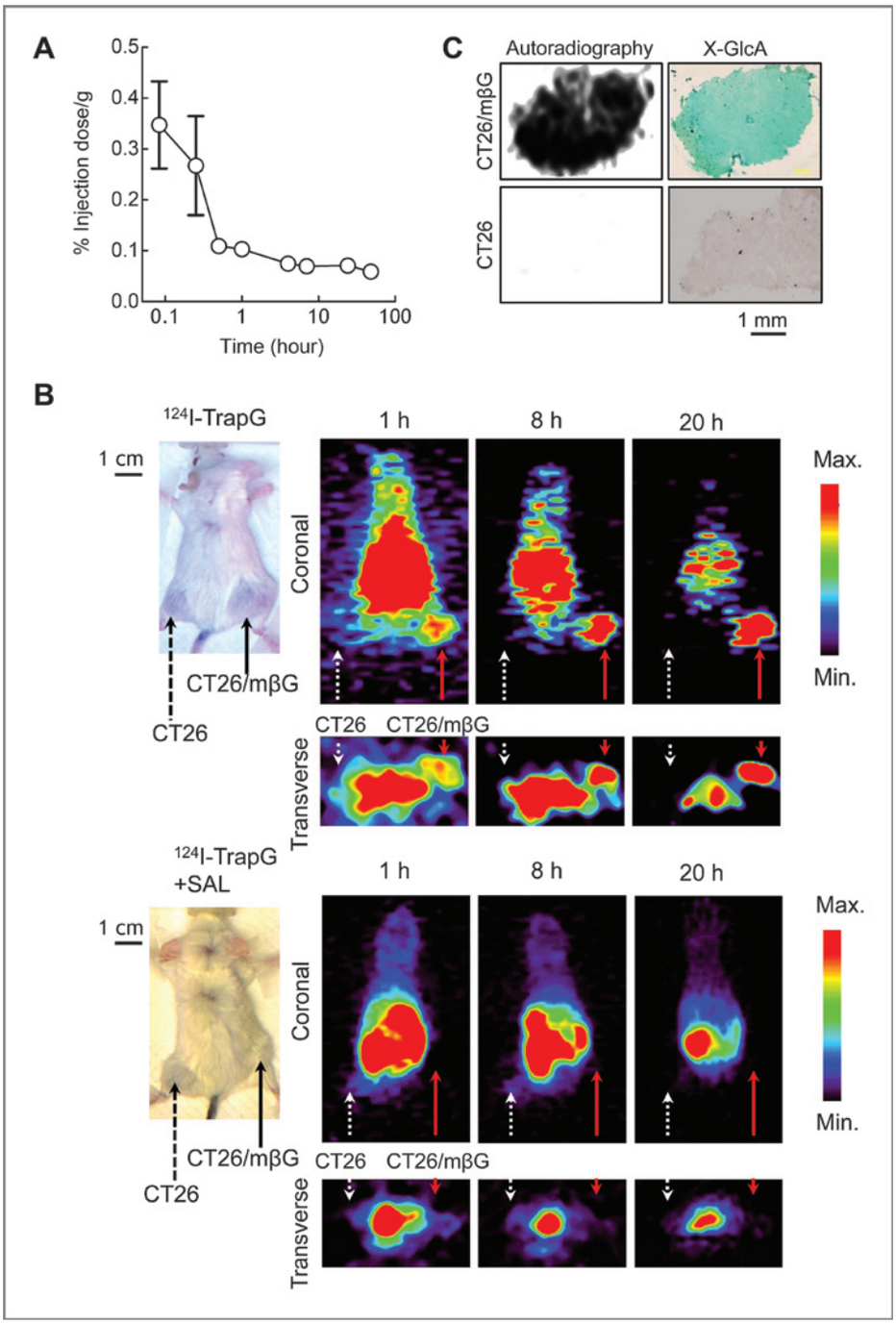

Figure 4. *In vivo* micro-PET imaging of βG by ^{124}I-TrapG. A, BALB/c mice ($n = 3$) were i.v. injected with 0.37 MBq of ^{124}I-TrapG. Serum samples were collected at the indicated times and directly measured on a gamma counter. The radioactivity in serum samples was expressed as a percentage of injected dose per gram tissue. Mean ± SD. B, BALB/c mice bearing CT26/mβG tumors (solid arrow) and control CT26 tumors (dashed arrow) were i.v. injected with 3.7 MBq of ^{124}I-TrapG in the presence or absence of SAL. Micro-PET images were acquired at the coronal and transverse planes of the mice at 1, 8, and 20 hours postinjection of the probe. Scale bar, 1 cm. C, CT26/mβG and CT26 tumors were resected at 20 hours after ^{124}I-TrapG injection for autoradiography (phosphor imaging) and βG activity (X-GlcA staining). Scale bar, 1 mm.

tumors but not CT26 tumors (Fig. 4B). The region of interest ratios of CT26/mβG to CT26 tumors were 3.3, 21, and 141.4 at 1, 8, and 20 hours, respectively, suggesting that ^{124}I-TrapG was preferentially hydrolyzed into ^{124}I-Trap by βG-mediated activation. The radioactivity accumulated in CT26/mβG tumors could last up to 20 hours, indicating that long-term imaging of βG activity can be achieved by using the βG-activated trapping ^{124}I-TrapG probe. To confirm whether conversion of ^{124}I-TrapG is βG dependent, mice bearing CT26/mβG and CT26 tumors were i.p. injected with the βG inhibitor SAL before probe injection for PET imaging. Figure 4B shows that SAL completely obstructed the generation and accumulation of radioactivity in CT26/mβG tumors, suggesting that the conversion of ^{124}I-TrapG to ^{124}I-Trap was blocked by the suppression of βG activity. A previous study showed that intraperitoneal administration of SAL in mice can prevent

Published OnlineFirst October 2, 2014; DOI: 10.1158/1535-7163.MCT-14-0212

CPT-11–induced mucosa damage by inhibiting bacterial βG (26). Although the pretreatment of SAL hampered the accumulation of cell-associated radioactivity in CT26/mβG tumors (Fig. 4B), strong abdominal signals were still observed. This result indicates that conversion of the fecal excreted ^{124}I-TrapG by intestinal βG is not the major source of the abdominal signals. To estimate the colocalization of βG activity and specific ^{124}I-TrapG retention, CT26 and CT26/mβG tumors were frozen, and sectioned 20 hours after the injection of ^{124}I-TrapG in tumor-bearing mice. The adjacent tumor sections were either directly exposed to phosphor imaging for autoradiography or stained with X-GlcA substrate to visualize βG activity. Figure 4C shows that autoradiography and βG activity matched in adjacent CT26/mβG tumor sections.

Biodistribution of the ^{131}I-TrapG in mice

To investigate the biodistribution of ^{131}I-TrapG *in vivo*, BALB/c mice ($n = 4$) bearing established CT26/mβG and CT26 tumors were i.v. injected with ^{131}I-TrapG and then examined by measuring radioactivity of the probe in organs at 1, 8, 20, and 40 hours after probe injection. Consistent with the micro-PET analysis, mean radioactivity of CT26/mβG tumors was significantly higher than the CT26 tumors (Fig. 5A). The accumulation of radioactivity in CT26/mβG tumors were 2.5-, 4.9-, 7.1-, and 9.60fold higher than the CT26 tumor at 1, 8, 20, and 40 hours, respectively. Notably, 15% and 15.7% of the total ^{131}I-TrapG were found in the gallbladder and urine, respectively, at 1 hour after injection (Fig. 5A). At 40 hours, 9.3% and 1.3% of the total ^{131}I-TrapG were found in the gallbladder and urine, respectively. This result suggests that ^{131}I-TrapG undergoes both renal and biliary excretion. ^{131}I-TrapG was eliminated rapidly by renal excretion but metabolized slowly by biliary excretion. To confirm this result, whole-mouse sections were detected by autoradiography at 40 hours after probe injection. Figure 5B shows that higher radioactivity accumulated in CT26/mβG tumors as compared with control CT26 tumors. However, we also found nontargeted ^{124}I-TrapG in the urine, gallbladder, liver, and intestines, which may be caused by the biliary excretion of ^{124}I-TrapG into the intestinal tract.

Imaging of βG activity in endogenous βG-overexpressing tumors for targeted 9ACG prodrug therapy

To further investigate whether TrapG probes can be used to image different levels of endogenous βG activity in tumors, mice bearing SW480, HCC36, CL1-5, SW620, Hela, or Colo205 tumors were i.v. injected with NIR-TrapG and imaged on an IVIS optical imaging system at 24 hours after injection. As shown in Fig. 6A and Supplementary Fig. S1, Colo205, CL1-5, and Hela (human βG^{high}) tumors displayed more fluorescence intensity than SW620, SW480, and HCC36 (human βG^{low}) tumors. These results suggest that TrapG probes can specifically image the different levels of βG activity in tumors. To investigate whether NIR-TrapG tumor imaging and 9ACG cancer therapy were contributed by increased βG in the tumor microenvironment, the mouse βG expression levels in human SW620 and Colo205 tumors were determined by reverse transcription PCR (RT-PCR). As shown in Fig. 6B, Colo205 tumors displayed elevated mouse βG as compared with the SW620 tumors, indicating that the conversion of TrapG probes and 9ACG prodrugs relies on extracellular βG in the tumor microenvironment. To

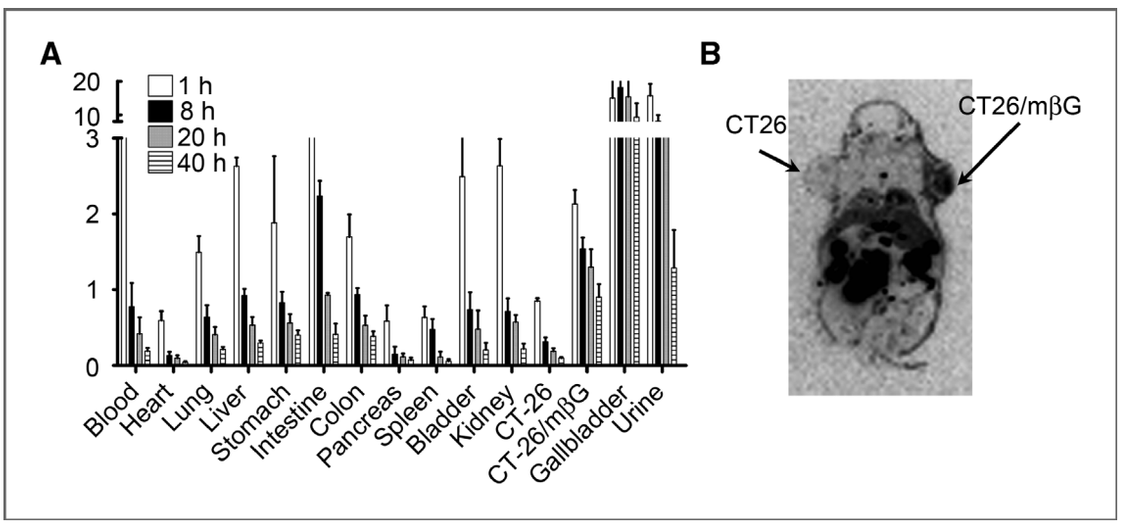

Figure 5. Biodistribution of ^{131}I-TrapG. BALB/c mice bearing CT26/mβG tumors and parental CT26 tumors were i.v. injected with 1.85 MBq of ^{131}I-TrapG. A, selected organs and tumors were harvested after 1 (white bars), 8 (black bars), 20 (gray bars), and 40 (hatched bars) hours. Radioactivity in the organs was measured by a gamma counter and normalized for sample weight. B, whole-body sections were detected by autoradiography (radioisotope image analyzer) at 40 hours after ^{131}I-TrapG injection. The biodistribution of ^{131}I-TrapG is expressed as a percentage of injected dose per gram tissue. Data, mean ± SD from 4 mice at each time point.

Published OnlineFirst October 2, 2014; DOI: 10.1158/1535-7163.MCT-14-0212

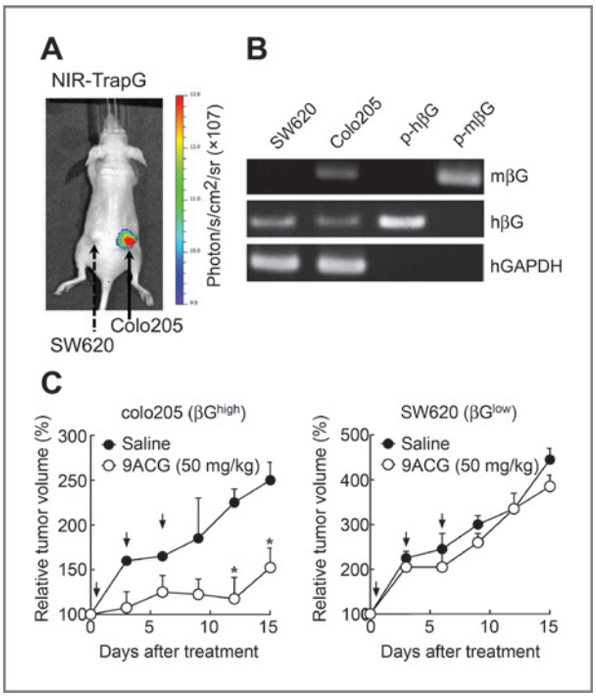

Figure 6. *In vivo* imaging of endogenous βG by TrapG probes for β-glucuronide prodrug therapy. A, BALB/c nude mice bearing SW620 and Colo205 tumors were i.v. injected with 100 μg of NIR-TrapG. Optical images were acquired at 24 hours postinjection of the probe. B, total RNA samples prepared from Colo205 and SW620 tumor tissue samples were used as templates for RT-PCR by using mouse βG (top), human βG (middle), or human GAPDH (bottom) gene-specific primers. The human GAPDH served as a loading control and the DNA plasmids containing mouse βG or human βG genes (p-mβG and p-hβG) served as positive controls. C, BALB/c nude mice bearing 100 mm^3 s.c. Colo205 (left) or SW620 (right) tumors were i.p. injected with PBS (●) or 50 mg/kg 9ACG (○) on days 1, 3, and 6. Bars, SEM ($n = 4$). Arrows, treatment schedule. Significant differences in mean tumor size in mice treated with 9ACG are indicated; *, $P < 0.05$.

estimate the antitumor potency of endogenous βG combined with 9ACG prodrug treatment, BALB/c nude mice bearing SW620 (human $βG^{low}$) or Colo205 (human $βG^{high}$) tumors were i.p. injected with PBS or 9ACG (50 mg/kg) on days 1, 3, and 6. 9ACG treatment significantly ($P < 0.05$) suppressed the growth of Colo205 tumors as compared with PBS treatment (Fig. 6C, left). In contrast, treatment of 9ACG in SW620 tumors did not significantly delay tumor growth (Fig. 6C, right). These results showed that the therapeutic efficacy of 9ACG prodrug is correlated with the expression levels of endogenous βG, thereby suggesting that the TrapG-based PET imaging system might be used to improve βG-mediated personalized antitumor treatments.

Discussion

We have successfully developed a ^{124}I-tyramine-difluoromethylphenol-glucuronide probe (^{124}I-TrapG) for *in vivo* monitoring of βG enzyme activity by micro-PET imaging. The *in vitro* and *in vivo* results demonstrated that the ^{124}I-TrapG probe can be activated by βG to radioactively image βG-expressing cells or tumors. In the cytotoxicity assay, native tyramine-TrapG displayed modest cytotoxicity in the presence of βG. We also found that the therapeutic efficacy of 9ACG prodrug is correlated to the βG levels in tumors that are determined by TrapG imaging. These results indicate that ^{124}I-TrapG may be a useful probe for the detection of βG activity by PET technology to optimize βG-based targeted therapies in the clinic.

Although ^{124}I-TrapG can be specifically converted by βG and thereby trapped in βG-expressing tumors, we also observed strong abdominal signals in mice. Two major causes may result in this background signals. First, liver cells can absorb xenobiotic glucuronides from the circulation by organic anion-transporting polypeptides such as estradiol-17-β-D-glucuronide and telmisartan acylglucuronide (27–29). Second, glucuronide conjugates can be transported to the intestines via biliary excretion. To diminish this effect, several methods have been used, including depletion of intestinal microbes by antibiotics (30, 31) and inhibition of bacterial βG by chemical inhibitors (32, 33). Therefore, we treated mice with antibiotics or a βG inhibitor before ^{124}I-TrapG injection. However, the abdominal signals were not reduced by either elimination of intestinal bacteria (data not show) or inhibition of bacterial βG activity (Fig. 4B). However, biliary excretion may be reduced by repeated injections of acetaminophen to induce Mrp3 expression and provoke the clearance of glucuronide conjugates through the urinary pathway (34).

βG is considered as a tumor marker (14, 15, 20) and a prodrug-activating enzyme for cancer prodrug therapies (35, 36). Connors and Whisson demonstrated that high βG levels present in plasmacytomas were correlated with higher drug sensitivity of the tumors (37). Indeed, we also found that Colo205 xenografts exhibited high levels of endogenous βG activity based on the imaging results using TrapG probes. Meanwhile, several studies have found that βG accumulates in the necrotic areas of human cancers (14, 18, 38, 39). In addition, glucuronide conjugates usually exhibit enhanced solubility and decreased cell permeability (3) that greatly increases the utility and specificity of prodrugs or proprobes relying on selective hydrolysis by the βG enzyme. Many βG activity–based prodrugs have been developed for cancer-targeted therapies, including 9ACG (24), BHAMG (40), daunorubicin-GA3 (DNR-GA3; ref. 35), and glucuronide-conjugated doxorubicin (DOX-GA3, HMR1826; ref. 35). Thus, the βG activity–based ^{124}I-TrapG imaging system may provide a powerful tool for tracking tumor associated βG activity by PET imaging to improve βG-based personalized anticancer therapies.

Development of a functional PET probe to image the βG activity in patients would improve βG-based targeted therapy. PET imaging is a sensitive, noninvasive, and clinical used technology for detecting organ function

Published OnlineFirst October 2, 2014; DOI: 10.1158/1535-7163.MCT-14-0212

and disease diagnosis. The high penetration of radioactive signals facilitates deep tissue/organ imaging (41, 42). Antunes and colleagues generated *1-O-(4-(2-^{18}fluoroethyl-carbamoyloxymethyl)-2-nitrophenyl)-O-β-D-glucopyronuronate* ([^{18}F]-FEAnGA) for *in vivo* tracking βG activity by PET imaging (43). However, the optimal radioactive accumulation of [^{18}F]-FEAnGA was 2-fold higher in βG-tumor than in control tumors at 1 hour (4). We have also previously developed a ^{124}I-labeled βG-based hydrophobic conversion probe (^{124}I-PTH-G) that can specifically accumulate at βG-expressing tumors. However, the optimal imaging efficiency of ^{124}I-PTH-G was only 3.6-fold greater in βG-expressing tumors than in control tumors at 1 hour (3). These studies indicate that both [^{18}F]-FEAnGA and ^{124}I-PTH-G rapidly diffuse away from βG-expressing sites and limit their utility for clinical use. In the present study, we describe a new ^{124}I-TrapG probe for monitoring of βG enzyme activity by micro-PET imaging. The optimal radioactive accumulation of ^{124}I-TrapG was 141.4-fold higher in βG-expressing tumors than in control tumors at 20 hours after probe injection. These results indicate that PET imaging of ^{124}I-TrapG is potentially useful for long-term monitoring of βG activity *in vivo*.

An imaging probe should display low toxicity, high specificity, and strong sensitivity. We previously demonstrated that a near infrared glucuronide trapping probe (NIR-TrapG) is an activity-based probe that allows specific and direct detection of βG activity in preclinical models (21). In addition, the glucuronide trapping probe did not inhibit βG enzyme activity, which can improve substrate activation, imaging intensity, and might not affect the conversion of βG-based prodrugs (43, 44). Here, we also verified that TrapG probe exhibits relatively low toxicity (IC_{50} > 200 μmol/L). In contrast, FIAU, the substrate for HSV-tk, is much more toxic (IC_{50} = 0.073 μmol/L; ref. 45). Moreover, the glucuronide trapping moiety (difluoromethylphenol) can be conjugated with various probes for multiimaging systems, such as fluorescent dyes (FITC and IR-820) for optical imaging (21) and radioactive isotopes (^{124}I) for micro-PET imaging. In the future, the glucuronide trapping probe could also be linked to clinical used diethylenetriamine pentaacetic acid (DTPA; ref. 46) for SPECT imaging or 1,4,7,10-tetraazacyclododecane-N,N′,N″,N‴-tetraacetic acid (DOTA; ref. 47), ultra-small paramagnetic iron oxide (USPIO) particles (48), and 1,4,7-tricarboxymethylene-1,4,7,10-tetraazacyclododecane (DO3A; ref. 49) for MR imaging. The ^{124}I-TrapG PET probe displays low toxicity, high sensitivity, noninhibition of enzyme activity, and long-term accumulation, which may facilitate monitoring βG activity in the clinical setting. Future developments to reduce the signals in the gastrointestinal tract should further refine and promote the use of the βG reporter system in the laboratory and clinical medicine.

The βG activity–based PET probe, ^{124}I-TrapG, is useful for noninvasive imaging of βG expression in the living body. The ^{124}I-TrapG possesses several advantages, including (i) the low toxicity of TrapG should allow clinical imaging, (ii) high specificity and signal amplification due to the catalytic hydrolysis of probes by βG, (iii) possibility of generating a wide range of imaging probes by attachment of TrapG groups, and (iv) retention of probes upon βG conversion leading to long-term imaging *in vivo*. On the basis of these advantages, ^{124}I-tyramine-TrapG may be paired with βG-based prodrugs to generate a personalized therapy system.

Disclosure of Potential Conflicts of Interest

No potential conflicts of interest were disclosed.

Authors' Contributions

Conception and design: Y.-C. Su, T.-C. Cheng, Y.-L. Leu, S.R. Roffler, H.-E. Wang, T.-L. Cheng
Development of methodology: Y.-C. Su, Y.-L. Leu, C.-H. Chuang, H.-E. Wang, T.-L. Cheng
Acquisition of data (provided animals, acquired and managed patients, provided facilities, etc.): Y.-C. Su, T.-C. Cheng, C.-H. Chuang, H.-E. Wang, T.-L. Cheng
Analysis and interpretation of data (e.g., statistical analysis, biostatistics, computational analysis): Y.-C. Su, T.-C. Cheng, J.-Y. Wang, H.-E. Wang, T.-L. Cheng
Writing, review, and/or revision of the manuscript: Y.-C. Su, T.-C. Cheng, S.R. Roffler, H.-E. Wang, T.-L. Cheng
Administrative, technical, or material support (i.e., reporting or organizing data, constructing databases): C.-H. Kao, K.-C. Chen, H.-E. Wang
Study supervision: H.-E. Wang, T.-L. Cheng

Acknowledgments

The authors thank Mr. Yen-Chen Lo of the Department of Biomedical Imaging and Radiological Sciences at National Yang Ming University, Taipei, Taiwan, for the production of ^{131}I-TrapG and ^{124}I-TrapG probes.

Grant Support

This study was supported by the National Research Program for Biopharmaceuticals, Ministry of Science and Technology, Taipei, Taiwan (MOST 103-2325-B-037-007 to T.-L. Cheng; MOST 103-2325-B-041-001, NSC 101-2320-B-041-001-MY2 to Y.-L. Leu); the Ministry of Health and Welfare, Taiwan (MOHW103-TD-B-111-05; to T.-L. Cheng); 103NSYSU-KMU Joint Research Project (NSYSUKMU103 I-003; to T.-L. Cheng); KMU-DT103005 (to T.-L. Cheng); the Center for Biomarkers and Biotech Drugs, Kaohsiung Medical University, Kaohsiung, Taiwan (KMU-TP103C00 and KMU-TP103H10; T.L. Cheng); and the Grant of Biosignature in Colorectal Cancers, Academia Sinica, Taiwan (to J.-Y. Wang and T.-L. Cheng).

The costs of publication of this article were defrayed in part by the payment of page charges. This article must therefore be hereby marked *advertisement* in accordance with 18 U.S.C. Section 1734 solely to indicate this fact.

Received March 10, 2014; revised August 29, 2014; accepted September 3, 2014; published OnlineFirst October 2, 2014.

References

1. Tomino S, Paigen K, Tulsiani DR, Touster O. Purification and chemical properities of mouse liver lysosomal (L form) beta-glucuronidase. J Biol Chem 1975;250:8503–9.
2. Su YC, Chuang KH, Wang YM, Cheng CM, Lin SR, Wang JY, et al. Gene expression imaging by enzymatic catalysis of a fluorescent probe via membrane-anchored beta-glucuronidase. Gene Ther 2007; 14:565–74.
3. Tzou SC, Roffler S, Chuang KH, Yeh HP, Kao CH, Su YC, et al. Micro-PET imaging of beta-glucuronidase activity by the hydrophobic conversion of a glucuronide probe. Radiology 2009;252:754–62.

Published OnlineFirst October 2, 2014; DOI: 10.1158/1535-7163.MCT-14-0212

4. Antunes IF, Haisma HJ, Elsinga PH, Dierckx RA, de Vries EF. Synthesis and evaluation of [18F]-FEAnGA as a PET Tracer for beta-glucuronidase activity. Bioconjug Chem 2010;21: 911–20.
5. Cheng TL, Chou WC, Chen BM, Chern JW, Roffler SR. Characterization of an antineoplastic glucuronide prodrug. Biochem Pharmacol 1999;58:325–8.
6. Heine D, Muller R, Brusselbach S. Cell surface display of a lysosomal enzyme for extracellular gene-directed enzyme prodrug therapy. Gene Ther 2001;8:1005–10.
7. Cheng CM, Lu YL, Chuang KH, Hung WC, Shiea J, Su YC, et al. Tumor-targeting prodrug-activating bacteria for cancer therapy. Cancer Gene Ther 2008;15:393–401.
8. Prijovich ZM, Chen KC, Roffler SR. Local enzymatic hydrolysis of an endogenously generated metabolite can enhance CPT-11 anticancer efficacy. Mol Cancer Ther 2009;8:940–6.
9. Cheng TL, Wei SL, Chen BM, Chern JW, Wu MF, Liu PW, et al. Bystander killing of tumour cells by antibody-targeted enzymatic activation of a glucuronide prodrug. Br J Cancer 1999;79:1378–85.
10. Chen BM, Cheng TL, Tzou SC, Roffler SR. Potentiation of antitumor immunity by antibody-directed enzyme prodrug therapy. Int J Cancer 2001;94:850–8.
11. Jeffrey SC, Nguyen MT, Moser RF, Meyer DL, Miyamoto JB, Senter PD. Minor groove binder antibody conjugates employing a water soluble beta-glucuronide linker. Bioorg Med Chem Lett 2007;17: 2278–80.
12. Weyel D, Sedlacek HH, Muller R, Brusselbach S. Secreted human beta-glucuronidase: a novel tool for gene-directed enzyme prodrug therapy. Gene Ther 2000;7:224–31.
13. Chen KC, Cheng TL, Leu YL, Prijovich ZM, Chuang CH, Chen BM, et al. Membrane-localized activation of glucuronide prodrugs by beta-glucuronidase enzymes. Cancer Gene Ther 2007;14:187–200.
14. Sperker B, Werner U, Murdter TE, Tekkaya C, Fritz P, Wacke R, et al. Expression and function of beta-glucuronidase in pancreatic cancer: potential role in drug targeting. Naunyn Schmiedebergs Arch Pharmacol 2000;362:110–5.
15. Juan TY, Roffler SR, Hou HS, Huang SM, Chen KC, Leu YL, et al. Antiangiogenesis targeting tumor microenvironment synergizes glucuronide prodrug antitumor activity. Clin Cancer Res 2009;15: 4600–11.
16. Banerjee SS, Aher N, Patil R, Khandare J. Poly(ethylene glycol)-prodrug conjugates: concept, design, and applications. J Drug Deliv 2012; 2012:103973.
17. Albin N, Massaad L, Toussaint C, Mathieu MC, Morizet J, Parise O, et al. Main drug-metabolizing enzyme systems in human breast tumors and peritumoral tissues. Cancer Res 1993;53:3541–6.
18. Schumacher U, Adam E, Zangemeister-Wittke U, Gossrau R. Histochemistry of therapeutically relevant enzymes in human tumours transplanted into severe combined immunodeficient (SCID) mice: nitric oxide synthase-associated diaphorase, beta-D-glucuronidase and non-specific alkaline phosphatase. Acta Histochem 1996;98:381–7.
19. Murdter TE, Sperker B, Kivisto KT, McClellan M, Fritz P, Friedel G, et al. Enhanced uptake of doxorubicin into bronchial carcinoma: beta-glucuronidase mediates release of doxorubicin from a glucuronide prodrug (HMR 1826) at the tumor site. Cancer Res 1997;57:2440–5.
20. Murdter TE, Friedel G, Backman JT, McClellan M, Schick M, Gerken M, et al. Dose optimization of a doxorubicin prodrug (HMR 1826) in isolated perfused human lungs: low tumor pH promotes prodrug activation by beta-glucuronidase. J Pharmacol Exp Ther 2002;301: 223–8.
21. Cheng TC, Roffler SR, Tzou SC, Chuang KH, Su YC, Chuang CH, et al. An activity-based near-infrared glucuronide trapping probe for imaging beta-glucuronidase expression in deep tissues. J Am Chem Soc 2012;134:3103–10.
22. National Toxicology P. NTP toxicology and carcinogenesis studies of phenolphthalein (CAS No. 77–09–8) in F344/N rats and B6C3F1 mice (feed studies). Natl Toxicol Program Tech Rep Ser 1996;465:1–354.
23. Janda KD, Lo LC, Lo CH, Sim MM, Wang R, Wong CH, et al. Chemical selection for catalysis in combinatorial antibody libraries. Science 1997;275:945–8.
24. Prijovich ZM, Chen BM, Leu YL, Chern JW, Roffler SR. Anti-tumour activity and toxicity of the new prodrug 9-aminocamptothecin glucuronide (9ACG) in mice. Br J Cancer 2002;86:1634–8.
25. Chu YW, Yang PC, Yang SC, Shyu YC, Hendrix MJ, Wu R, et al. Selection of invasive and metastatic subpopulations from a human lung adenocarcinoma cell line. Am J Respir Cell Mol Biol 1997;17: 353–60.
26. Fittkau M, Voigt W, Holzhausen HJ, Schmoll HJ. Saccharic acid 1.4-lactone protects against CPT-11-induced mucosa damage in rats. J Cancer Res Clin Oncol 2004;130:388–94.
27. Ishiguro N, Maeda K, Saito A, Kishimoto W, Matsushima S, Ebner T, et al. Establishment of a set of double transfectants coexpressing organic anion transporting polypeptide 1B3 and hepatic efflux transporters for the characterization of the hepatobiliary transport of telmisartan acylglucuronide. Drug Metab Dispos 2008;36: 796–805.
28. Kanai N, Lu R, Bao Y, Wolkoff AW, Vore M, Schuster VL. Estradiol 17 beta-D-glucuronide is a high-affinity substrate for oatp organic anion transporter. Am J Physiol 1996;270:F326–31.
29. Shitara Y, Li AP, Kato Y, Lu C, Ito K, Itoh T, et al. Function of uptake transporters for taurocholate and estradiol 17beta-D-glucuronide in cryopreserved human hepatocytes. Drug Metab Pharmacokinet 2003;18:33–41.
30. Kehrer DF, Sparreboom A, Verweij J, de Bruijn P, Nierop CA, van de Schraaf J, et al. Modulation of irinotecan-induced diarrhea by cotreatment with neomycin in cancer patients. Clin Cancer Res 2001;7:1136–41.
31. Takasuna K, Hagiwara T, Watanabe K, Onose S, Yoshida S, Kumazawa E, et al. Optimal antidiarrhea treatment for antitumor agent irinotecan hydrochloride (CPT-11)-induced delayed diarrhea. Cancer Chemother Pharmacol 2006;58:494–503.
32. Wallace BD, Wang H, Lane KT, Scott JE, Orans J, Koo JS, et al. Alleviating cancer drug toxicity by inhibiting a bacterial enzyme. Science 2010;330:831–5.
33. Alimonti A, Gelibter A, Pavese I, Satta F, Cognetti F, Ferretti G, et al. New approaches to prevent intestinal toxicity of irinotecan-based regimens. Cancer Treat Rev 2004;30:555–62.
34. Ghanem CI, Ruiz ML, Villanueva SS, Luquita MG, Catania VA, Jones B, et al. Shift from biliary to urinary elimination of acetaminophen-glucuronide in acetaminophen-pretreated rats. J Pharmacol Exp Ther 2005;315:987–95.
35. de Graaf M, Boven E, Scheeren HW, Haisma HJ, Pinedo HM. Beta-glucuronidase-mediated drug release. Curr Pharm Des 2002;8:1391–403.
36. Chen X, Wu B, Wang PG. Glucuronides in anti-cancer therapy. Curr Med Chem Anticancer Agents 2003;3:139–50.
37. Connors TA, Whisson ME. Cure of mice bearing advanced plasma cell tumours with aniline mustard: the relationship between glucuronidase activity and tumour sensitivity. Nature 1966;210:866–7.
38. Bosslet K, Straub R, Blumrich M, Czech J, Gerken M, Sperker B, et al. Elucidation of the mechanism enabling tumor selective prodrug monotherapy. Cancer Res 1998;58:1195–201.
39. Houba PH, Boven E, van der Meulen-Muileman IH, Leenders RG, Scheeren JW, Pinedo HM, et al. A novel doxorubicin-glucuronide prodrug DOX-GA3 for tumour-selective chemotherapy: distribution and efficacy in experimental human ovarian cancer. Br J Cancer 2001;84:550–7.
40. Wang SM, Chern JW, Yeh MY, Ng JC, Tung E, Roffler SR. Specific activation of glucuronide prodrugs by antibody-targeted enzyme conjugates for cancer therapy. Cancer Res 1992;52:4484–91.
41. Hung SC, Deng WP, Yang WK, Liu RS, Lee CC, Su TC, et al. Mesenchymal stem cell targeting of microscopic tumors and tumor stroma development monitored by noninvasive *in vivo* positron emission tomography imaging. Clin Cancer Res 2005;11:7749–56.
42. Kelloff GJ, Krohn KA, Larson SM, Weissleder R, Mankoff DA, Hoffman JM, et al. The progress and promise of molecular imaging probes in oncologic drug development. Clin Cancer Res 2005;11:7967–85.
43. Antunes IF, Doorduin J, Haisma HJ, Elsinga PH, van Waarde A, Willemsen AT, et al. 18F-FEAnGA for PET of beta-glucuronidase activity in neuroinflammation. J Nucl Med 2012;53:451–8.
44. Blum G, Weimer RM, Edgington LE, Adams W, Bogyo M. Comparative assessment of substrates and activity based probes as tools for non-

Published OnlineFirst October 2, 2014; DOI: 10.1158/1535-7163.MCT-14-0212

invasive optical imaging of cysteine protease activity. PLoS ONE 2009;4:e6374.

45. Ashida N, Watanabe Y, Miura S, Kano F, Sakata S, Yamaguchi T, et al. Structure-activity relationship of the affinity of 5-substituted uracil nucleoside analogues for varicella-zoster virus thymidine kinase and their activity against varicella-zoster virus. Antiviral Res 1997;35: 167–75.
46. Patil RR, Yu J, Banerjee SR, Ren Y, Leong D, Jiang X, et al. Probing *in vivo* trafficking of polymer/DNA micellar nanoparticles using SPECT/CT imaging. Mol Ther 2011;19:1626–35.
47. Cai W, Rao J, Gambhir SS, Chen X. How molecular imaging is speeding up antiangiogenic drug development. Mol Cancer Ther 2006;5:2624–33.
48. Raty JK, Liimatainen T, Unelma Kaikkonen M, Grohn O, Airenne KJ, Yla-Herttuala S. Non-invasive imaging in gene therapy. Mol Ther 2007;15:1579–86.
49. Bohndiek SE, Kettunen MI, Hu DE, Witney TH, Kennedy BW, Gallagher FA, et al. Detection of tumor response to a vascular disrupting agent by hyperpolarized 13C magnetic resonance spectroscopy. Mol Cancer Ther 2010;9:3278–88.